Universal Instability for Wavelengths below the Ion Larmor Scale

Matt Landreman,* Thomas M. Antonsen, Jr., and William Dorland
Institute for Research in Electronics and Applied Physics, University of Maryland, College Park, Maryland 20742, USA
(Received 6 November 2014; published 4 March 2015)

We demonstrate that the universal mode driven by the density gradient in a plasma slab can be absolutely unstable even in the presence of reasonable magnetic shear. Previous studies from the 1970s that reached the opposite conclusion used an eigenmode equation limited to $L_x \gg \rho_i$, where L_x is the scale length of the mode in the radial direction, and ρ_i is the ion Larmor radius. Here we instead use a gyrokinetic approach which does not have this same limitation. Instability is found for perpendicular wave numbers k_y in the range $0.7 \lesssim k_y\rho_i \lesssim 100$, and for sufficiently weak magnetic shear: $L_s/L_n \gtrsim 17$, where L_s and L_n are the scale lengths of magnetic shear and density. Thus, the plasma drift wave in a sheared magnetic field may be unstable even with no temperature gradients, no trapped particles, and no magnetic curvature.

DOI: 10.1103/PhysRevLett.114.095003 PACS numbers: 52.35.Kt, 52.65.Tt

Introduction.—Following a series of papers in 1978 [1–3], it has been widely accepted that drift waves in a plasma in a sheared magnetic field, in the absence of parallel current, temperature gradients, and magnetic curvature, are absolutely stable. In other words, the "universal mode" driven by the density gradient in slab geometry [4,5] becomes absolutely stable if any magnetic shear is included. This conclusion is important as a basic problem of plasma physics, and for understanding the physical mechanisms underlying instabilities in more complicated configurations in laboratory or space plasmas. For example, the slab limit can provide insight into the edge of magnetically confined plasmas, in which the slablike drive from radial equilibrium gradients ($\sim 1/L_\perp$ for scale length $L_\perp$) exceeds the curvature drive ($\sim 1/R$ for major radius R), and in which the temperature gradient may tend to be relatively weaker than the density gradient since the former is more strongly equilibrated over ion orbits [6]. However, in contrast to the 1978 work (and later studies [7,8]), here we demonstrate that the universal mode is in fact unstable for a range of perpendicular wave numbers k_y satisfying $k_y\rho_i \gtrsim 0.7$, where ρ_i is the ion gyroradius. We reach a different conclusion than the 1978 work because these earlier calculations relied on an eigenmode equation derived under the assumption $L_x \gg \rho_i$, where L_x is the radial scale length of the fluctuating mode in untwisted coordinates. In contrast, our gyrokinetic approach does not share this limitation.

Gyrokinetic model.—In slab geometry with magnetic shear, the magnetic field in Cartesian coordinates $(\hat{x}, \hat{y}, \hat{z})$ is $\boldsymbol{B} = [\boldsymbol{e}_{\hat{z}} + (\hat{x}/L_s)\boldsymbol{e}_{\hat{y}}]B$ for some constant B and shear length L_s. A field-aligned coordinate system is introduced: $x = \hat{x}$, $y = \hat{y} - \hat{x}\,\hat{z}\,/L_s$, $z = \hat{z}$, so $\boldsymbol{B}\cdot\nabla x = \boldsymbol{B}\cdot\nabla y = 0$ and $\boldsymbol{B}\cdot\nabla z = B$. We consider electrostatic fluctuations satisfying the standard gyrokinetic orderings [9–11]: the gyroradii are of the same formal order as the perpendicular wavelengths of the fluctuations, and these scales are 1 order smaller than the scale lengths of the equilibrium density and magnetic field. We therefore may use the linear electrostatic gyrokinetic and quasineutrality equations derived in [9–11], dropping toroidal effects, temperature gradients, and collisions (except where noted in Fig. 4.) For perturbations varying in y as $\exp(ik_y y)$ and independent of x, the gyrokinetic equation is

$$\frac{\partial h_s}{\partial t} + v_{\parallel}\frac{\partial h_s}{\partial z} = \frac{q_s}{T_s} f_{Ms} J_{0s}\frac{\partial \Phi}{\partial t} - \frac{ik_y f_{Ms}}{BL_n} J_{0s}\Phi, \quad (1)$$

and the quasineutrality condition is

$$\sum_s \left[-\frac{q_s^2 n_s \Phi}{T_s} + q_s \int d^3 v J_{0s} h_s\right] = 0. \quad (2)$$

Here, $s \in \{i, e\}$ denotes species, $\Phi(t, z)$ is the electrostatic potential, $h_s(t, z, \mathcal{E}, \mu)$ is the nonadiabatic distribution function, $\mathcal{E} = v^2/2$, $\mu = v_\perp^2/(2B)$, and f_{Ms} is the leading-order Maxwellian. The scale length of the equilibrium electron density $n = n_e$ is $L_n = -n/(dn/dx)$, $q_i = e = -q_e$ is the proton charge, T_s is the species temperature, $J_{0s}(z) = J_0(k_\perp v_\perp/\Omega_s)$, $k_\perp(z) = k_y\sqrt{1 + (z/L_s)^2}$, $\Omega_s = q_s B/m_s$, and J_0 is a Bessel function. As $k_y\rho_i$ was ordered ~ 1, Eqs. (1) and (2) are valid for both $k_y\rho_i \geq 1$ and ≤ 1; the same is true of $k_y\rho_e$, where ρ_e is the electron gyroradius.

For eigenmodes $\propto \exp(-i\omega t)$, a dispersion equation can be obtained by introducing $\hat{\Phi}(x)$ satisfying

$$\Phi(z) = \int dx\, \hat{\Phi}(x) \exp\left(\frac{ik_y x z}{L_s}\right), \quad (3)$$

with an analogous transform for h_s. We use $x = \hat{x}$ as the transform variable because $\hat{\Phi}(x)$ represents the radial mode in the untwisted coordinates. Using (3), $\partial/\partial z$ in (1) becomes $ik_\parallel = ik_y x/L_s$, so (1) may be solved for $\hat{h}_s$. Using (2) and approximating $J_{0e} \approx 1$, we obtain [8]

$$0 = \left[\frac{T_e}{T_i} + 1 + \left(1 - \frac{\omega_*}{\omega}\right)\left|\frac{L_s}{k_y x}\right|\frac{\omega}{v_e} Z\left(\left|\frac{L_s}{k_y x}\right|\frac{\omega}{v_e}\right)\right]\hat{\Phi}(x) + \left(\frac{T_e}{T_i} + \frac{\omega_*}{\omega}\right)\left(\frac{k_y}{2\pi L_s}\right)^2 \int dx' \int dx'' \int dz \int dz' \times \Gamma_{0i}(z, z')\hat{\Phi}(x'') \exp\left(\frac{ik_y}{L_s}[x'z - x'z' - xz + x''z']\right) \times \left|\frac{L_s}{k_y x'}\right|\frac{\omega}{v_i} Z\left(\left|\frac{L_s}{k_y x'}\right|\frac{\omega}{v_i}\right), \quad (4)$$

where

$$\Gamma_{0i}(z, z') = I_0\left(\frac{k_y^2\rho_i^2}{2}\sqrt{1 + \frac{z^2}{L_s^2}}\sqrt{1 + \frac{z'^2}{L_s^2}}\right) \times \exp\left(-\frac{k_y^2\rho_i^2}{4}\left[2 + \frac{z^2 + z'^2}{L_s^2}\right]\right). \quad (5)$$

Here, $v_s = \sqrt{2T_s/m_s}$, $\rho_i = v_i/\Omega_i$, I_0 is a modified Bessel function, Z is the plasma dispersion function, and $\omega_* = k_y T_e/(eBL_n)$ is the drift frequency. The multiple Fourier transforms in Eq. (4) arise because the Z function arguments are naturally written in terms of $k_{||} \propto x$, whereas the Bessel function arguments are naturally written in terms of z. Notice the integral equation (4) from this gyrokinetic approach is manifestly different from the differential eigenmode equations in Refs. [1–3].

Numerical demonstration of instability.—We solve Eqs. (1) and (2) using two independent codes, GS2 [12] and GENE [13–15]. A demonstration of linear instability is given in Fig. 1 for $L_s/L_n = 32$. In this figure and hereafter, $T_i = T_e$. Because of the literature asserting stability, we have taken great care to verify that this instability is robust and not a numerical artifact. To this end, we demonstrate in Fig. 1 precise agreement between the two codes, which use different velocity-space coordinates and different numerical algorithms. The figure shows calculations from GS2 run as initial-value simulations, and from GENE run as a direct eigenmode solver using the SLEPc library [16]. For each code, results are plotted for many different resolutions to demonstrate convergence. (For GS2, results are overlaid for 8 sets of numerical parameters: a base resolution, 2× number of parallel grid points, 3× parallel box size, 2× number of energy grid points, 2× maximum energy, 2× number of pitch angle grid points, 1/2 time step, and 2× maximum time. For GENE, results are again overlaid for 8 sets of numerical parameters: a base resolution, 2× number of parallel grid points, 2× parallel box size, 2× number of $v_\perp$ grid points, 2× maximum perpendicular energy, 2× number of $v_{||}$ grid points, 2× maximum parallel energy, and 2× numerical hyperviscosity.) To further minimize the possibility of numerical artifacts, for this figure a reduced mass ratio $m_i/m_e = 25$ was employed. As the differences between the 16 series displayed in each plot are nearly invisible, the instability is clearly physical and not numerical.

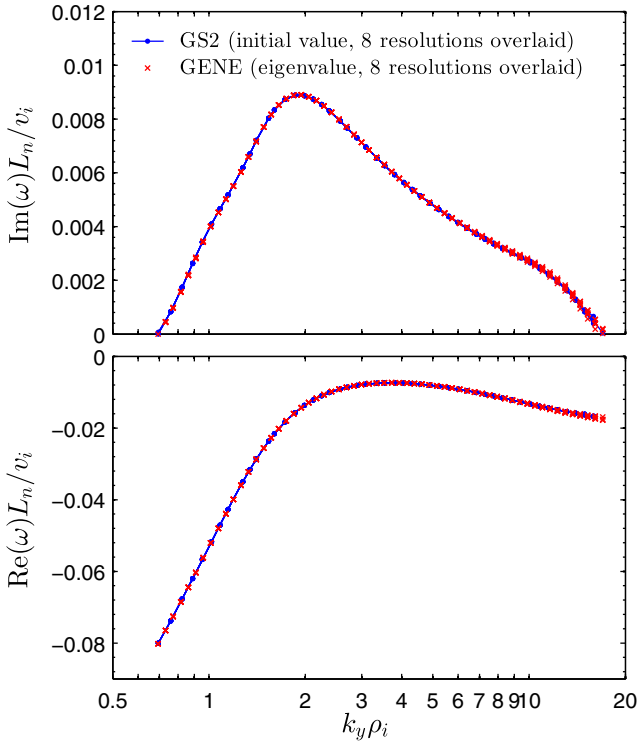

FIG. 1 (color online). Demonstration that the universal instability is numerically robust. The positive growth rate and real frequency are plotted for the unstable range of k_y using calculations from two independent codes—GS2 run as an initial-value simulation and GENE run as a direct eigenvalue solver—with results agreeing to high precision. For each code, results from many different numerical resolutions are overlaid in the figure. A reduced mass ratio $m_i/m_e = 25$ is used here to further minimize the possibility of numerical artifacts.

Mode properties.—Figure 2 displays the dependence of the frequency and growth rate on perpendicular wave number and magnetic shear, this time using the true deuterium-electron mass ratio. As one expects from the zero-shear universal instability, the phase velocity direction is $\mathrm{Re}(\omega/\omega_*) > 0$ [appearing in the figures as $\mathrm{Re}(\omega) < 0$ due to the codes' sign convention]. The frequency satisfies $|\omega L_n/v_i| \ll 1$ and $|\omega/\omega_*| \ll 1$. The growth rate is smaller in magnitude than the real frequency.

When $L_s/L_n \gg 1$, instability is found for $k_y\rho_i > 0.7$, extending beyond $k_y\rho_i > 100$ for the highest values of L_s/L_n. Stability for $k_y \to \infty$ can be understood from the fact that J_{0s} in Eqs. (1) and (2) becomes small, as the gyromotion averages out very small-scale fluctuations. Stability in the opposite limit of small k_y is expected since Refs. [1,2] are valid there. A region of stability also exists around $k_y\rho_i \approx 2$ when a realistic mass ratio is used. No such notch in the growth rate is found when the shear is exactly zero. This abrupt change in eigenvalue when a small change is made to the physical system—in this case the

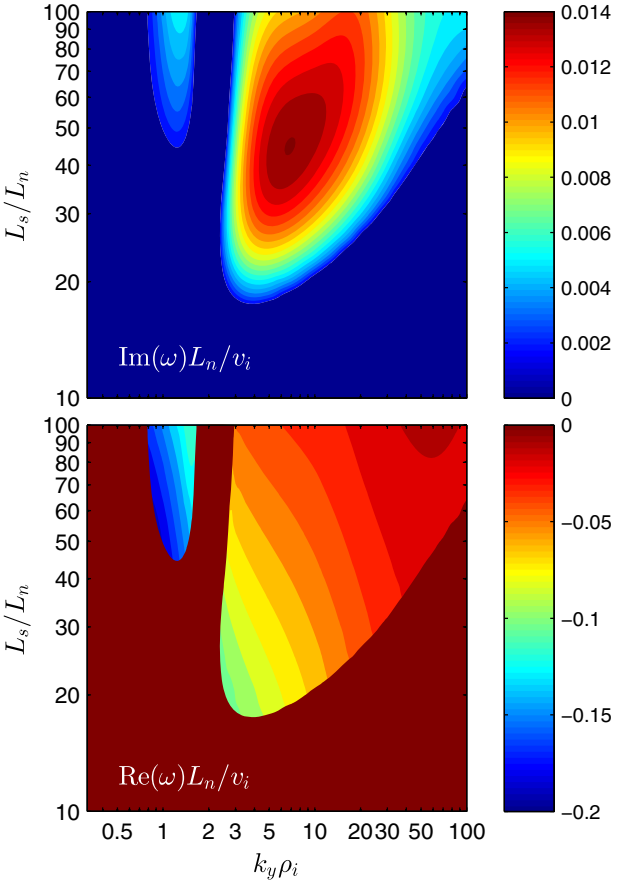

FIG. 2 (color online). Dependence of the universal instability on wave number and magnetic shear, for $m_i/m_e = 3600$. Calculations are performed with the GS2 code.

addition of small magnetic shear for $k_y\rho_i \approx 2$—is a phenomenon seen in many systems with nonorthogonal eigenmodes [17] such as this one. For such "non-normal" systems, the behavior over a finite time is typically a much less sensitive function of parameters than the eigenvalues, which represent behavior for $t \to \infty$ when all points along the field line have had time to communicate. Indeed, in initial-value computations we find no notch near $k_y\rho_i \approx 2$ in the growth for short times $t \lesssim L_s/v_i$, before ions have traveled far enough in z to "realize" there is shear; these results will be presented in a separate publication.

Instability is found for at least some values of k_y whenever L_s/L_n exceeds a critical value of ~17. Note that in a tokamak, $L_s/L_n \approx qR/(\hat{s}L_n) \gg 1$ can exceed this threshold value. Here q is the safety factor, R is the major radius, $\hat{s} = (r/q)dq/dr$, and r is the minor radius. The general trend in Fig. 2 of decreasing growth rate with increasing shear can be understood from the observation that in the zero-shear limit, instability is found when $|k_{||}|$ is below a $k_\perp$-dependent threshold. When sufficient shear is included, all of these unstable parallel wavelengths are sufficiently long for there to be a significant increase in $k_\perp = k_y\sqrt{1 + (z/L_s)^2}$, causing Φ to be averaged out by gyroaveraging as discussed above. For some $k_y\rho_i$ such as ~7, the growth rate does not increase monotonically with L_s/L_n. This effect is another example of eigenvalues being sensitive and perhaps misleading, typical in non-normal systems [17] such as this one, for we find the short-time amplification to increase with L_s/L_n monotonically.

A typical unstable eigenmode is shown in Fig. 3. This example is obtained using GS2 at $L_s/L_n = 50$ and $k_y\rho_i = 10$, near the maximum growth rate in Fig. 2. In the field-aligned parallel coordinate z, the mode has a parallel extent $\sim L_s$. Fourier transforming, the extent of the radial eigenmode is $\lesssim\rho_i$. Most of the mode structure occurs where the ion Z function has an argument of order 1, $|x| \sim |\omega L_s/(k_y v_i)|$, so the electron Z function has small argument. The eigenmode amplitude is small in the inner electron region where $|x| < |\omega L_s/(k_y v_e)|$. The electrons are highly nonadiabatic: noting the ratio of electron nonadiabatic/adiabatic terms in Eq. (4) is $\approx -(i\sqrt{\pi}/2)(L_s/L_n)(\rho_e/\rho_i)(\rho_i/|x|)$, then the nonadiabatic electron term exceeds the adiabatic term wherever $|x| < 0.7\rho_i$, everywhere the eigenfunction is significant.

Dependence of the instability on temperature gradients and collisionality is shown in Fig. 4, for the case $L_s/L_n = 50$ and $m_i/m_e = 3600$. Collisions (using the operator in [18]) reduce the growth rate, particularly at the highest k_y values. This behavior is expected because (i) in the free energy moment of Eq. (1) [Eq. (222) of [19]] collisions provide an energy sink, (ii) the gyrokinetic collision operator [18] contains terms $\propto k_\perp^2$, and (iii) the modes at highest k_y have fine velocity-space structure (as high resolution in energy and pitch angle is required

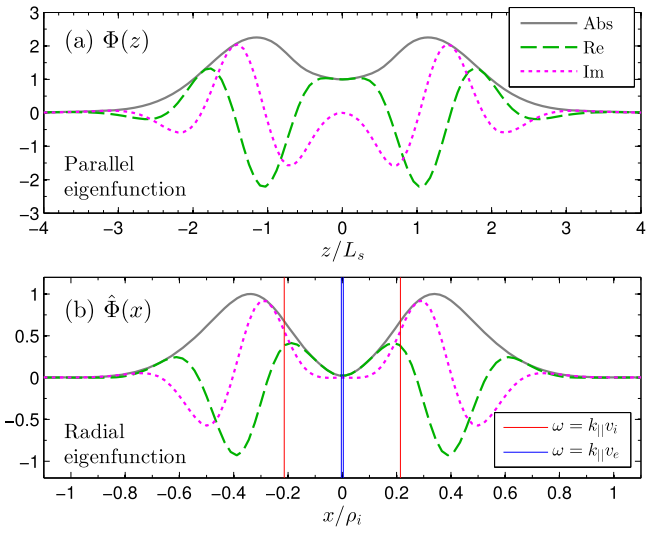

FIG. 3 (color online). Eigenmode computed with GS2 for $L_s/L_n = 50$, $m_i/m_e = 3600$, and $k_y\rho_i = 10$ (near the maximum growth rate in Fig. 2). In (b), noting $k_{||} = k_y x/L_s$, vertical lines indicate the values of x at which the arguments of the electron and ion Z functions in Eq. (4) have unit magnitude. (a) Parallel eigenfunction $\Phi(z)$ and (b) Radial eigenfunction $\hat{\Phi}(x)$.

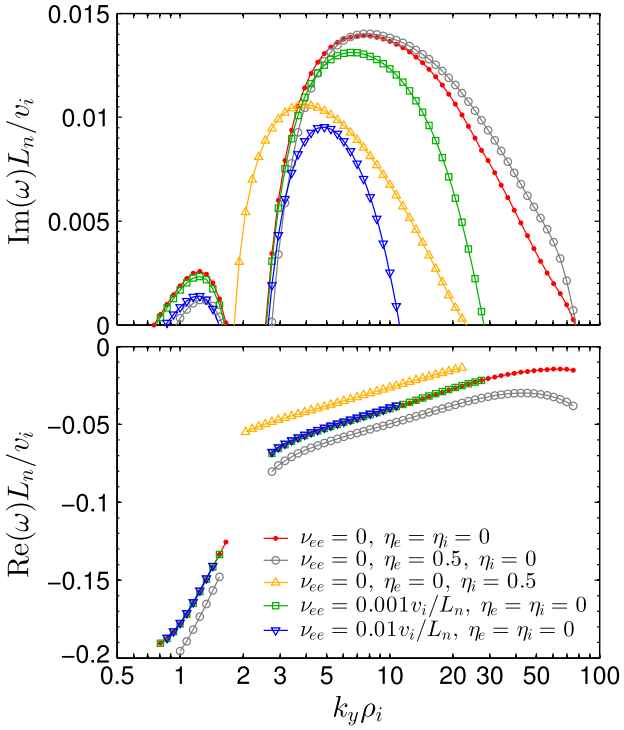

FIG. 4 (color online). Growth rate and real frequency vs wave number for $L_s/L_n = 50$ and $m_i/m_e = 3600$, showing trends with $\eta_s = (d\ln T_s/dx)/(d\ln n_s/dx)$ and collisionality.

for numerical convergence), which collisions destroy. For sufficient collisionality, $\nu_{ee} \sim 0.05 v_i/L_n$ or more, the mode is stabilized at all k_y (for this L_s/L_n).

Relationship to previous work.—Let us now examine in greater detail why we find instability whereas previous authors found stability. First, consider Ref. [3], which gave an analytical proof of stability in the limit $T_i \ll T_e$. We find no contradiction using gyrokinetic simulations, obtaining instability only when T_i/T_e is not small. (Recall $T_i = T_e$ for all figures here.)

Next, consider Refs. [1,2]. These authors considered a differential eigenvalue equation, not equivalent to Eq. (4), derived assuming

$$\rho_i^2 |\hat{\Phi}^{-1} \partial^2 \hat{\Phi}/\partial x^2| \ll 1; \tag{6}$$

see, e.g., [20]. No such assumption was made in deriving Eq. (4), which is therefore more general. Considering the typical eigenmode in Fig. 3(b), there is structure on scales smaller than ρ_i, violating Eq. (6). Therefore, the approach used in Refs. [1,2] is inapplicable for the modes that are unstable.

Reference [7] claims to give a proof of stability which does not rely on (6). However, this reference uses an integral eigenmode equation which differs from Eq. (4), so it is not surprising that we reach different conclusions. The eigenmode equation in Ref. [7] is effectively a WKB approximation, the zero-shear dispersion relation but with k_x replaced by $-id/dx$. This WKB approximation is not justified for modes such as the one in Fig. 3, in which the wavelengths in x are comparable to or much longer than the scale of variation in the ion and electron Z functions. The problems with the integral equation in Ref. [7] are discussed in the introduction of Ref. [8] and references therein.

Reference [8] appears to give a proof of stability using the full gyrokinetic integral eigenmode Eq. (4). Although we retain J_{0e} for all numerical results shown here while J_{0e} is set to 1 in Ref. [8], this difference is unimportant: we find little change in the instability for $k_y\rho_i < 20$ if J_{0e} is set to 1 in GS2. The proof in Ref. [8] is accomplished by multiplying the electron nonadiabatic term in Eq. (4) ($\propto 1 - \omega_*/\omega$) by a parameter λ. The authors first prove stability in the adiabatic electron limit $\lambda = 0$. We do not disagree, as we find no instability numerically with adiabatic electrons. However, we do disagree with the final step of the proof, where it is argued that solutions for ω cannot cross the real axis as λ is increased from 0 to 1 to recover Eq. (4). Including λ in GS2, we find that modes do continuously transform from damped to unstable as λ is increased from 0 to 1. For the case $L_s/L_n = 50$ and $k_y\rho_i = 10$ shown in Fig. 3, marginal stability occurs when $\lambda = 0.032$. Therefore, the problematic step in Ref. [8] is item (iii) on p750. Indeed, when $\lambda > 0$, a nonadiabatic electron term must be included in (38)–(55), and this term can have opposite sign to the other terms in (55), so (56) no longer follows.

Conclusions.—In summary, we find the plasma slab with weak or moderate magnetic shear ($L_s/L_n > 17$) is generally unstable at low collisionality, even when temperature gradients are weak. The density-gradient-driven electron drift wave, known to be absolutely unstable in the absence of magnetic shear [4,5], is not stabilized at all wavelengths when small magnetic shear is introduced, counter to previous findings. This instability is seen robustly in multiple gyrokinetic codes, and occurs for $k_y\rho_i \gtrsim 1$. Previous work that apparently showed stability of the universal mode [1–3] assumed either Eq. (6) or $T_i \ll T_e$, whereas we make neither assumption. Reference [7] employed a less accurate dispersion relation, and Ref. [8] appears incorrect for nonadiabatic electrons. Though it has sometimes been assumed that an electrostatic instability seen in a gyrokinetic simulation propagating in the electron diamagnetic direction must be a trapped electron mode or electron temperature gradient mode, our results indicate neither trapped particles nor temperature gradients are necessary for instability in this phase-velocity direction. As the universal mode can indeed be absolutely unstable in the presence of magnetic shear, it should be considered alongside temperature-gradient-driven modes, trapped particle instabilities, ballooning modes, and tearing modes as one of the fundamental plasma microinstabilities.

This material is based upon work supported by the U.S. Department of Energy, Office of Science, Office of Fusion Energy Science, under Awards No. DEFG0293ER54197 and No. DEFC0208ER54964 and the SciDAC Center for the Study of Plasma Microturbulence. Computations were performed on the Edison system at the National Energy Research Scientific Computing Center, a DOE Office of Science User Facility supported by the Office of Science of the U.S. Department of Energy under Contract No. DE-AC02-05CH11231. We wish to thank Tobias Görler for providing the GENE code. We also acknowledge conversations about this work with Peter Catto, Greg Hammett, Adil Hassam, Edmund Highcock, Wrick Sengupta, Jason TenBarge, and George Wilkie.

*mattland@umd.edu

[1] D. W. Ross and S. M. Mahajan, Phys. Rev. Lett. **40**, 324 (1978).
[2] K. T. Tsang, P. J. Catto, J. C. Whitson, and J. Smith, Phys. Rev. Lett. **40**, 327 (1978).
[3] T. M. Antonsen, Jr., Phys. Rev. Lett. **41**, 33 (1978).
[4] A. A. Galeev, V. N. Oraevsky, and R. Z. Sagdeev, J. Exptl. Theoret. Phys. **44**, 903 (1963) [JETP Lett. Sov. Phys. JETP **17**, 615 (1963)].
[5] N. A. Krall and M. N. Rosenbluth, Phys. Fluids **8**, 1488 (1965).
[6] G. Kagan and P. J. Catto, Plasma Phys. Controlled Fusion **50**, 085010 (2008).
[7] Y. C. Lee, L. Chen, and W. M. Nevins, Nucl. Fusion **20**, 482 (1980).
[8] L. Chen, F. J. Ke, M. J. Xu, S. T. Tsai, Y. C. Lee, and T. M. Antonsen, Jr., Plasma Phys. **24**, 743 (1982).
[9] P. H. Rutherford and E. A. Frieman, Phys. Fluids **11**, 569 (1968).
[10] J. B. Taylor and R. J. Hastie, Plasma Phys. **10**, 479 (1968).
[11] P. J. Catto, Plasma Phys. **20**, 719 (1978).
[12] M. Kotschenreuther, G. Rewoldt, and W. M. Tang, Comput. Phys. Commun. **88**, 128 (1995).
[13] F. Jenko, W. Dorland, M. Kotschenreuther, and B. N. Rogers, Phys. Plasmas **7**, 1904 (2000).
[14] T. Dannert and F. Jenko, Phys. Plasmas **12**, 072309 (2005).
[15] T. Görler, X. Lapillonne, S. Brunner, T. Dannert, F. Jenko, F. Merz, and D. Told, J. Comput. Phys. **230**, 7053 (2011).
[16] V. Hernandez, J. E. Roman, and V. Vidal, ACM Trans. Math. Softw. **31**, 351 (2005).
[17] L. Trefethen and M. Embree, *Spectra and Pseudospectra: The Behavior of Nonnormal Matrices and Operators* (Princeton University Press, Princeton, NJ, 2005).
[18] I. G. Abel, M. Barnes, S. C. Cowley, W. Dorland, and A. A. Schekochihin, Phys. Plasmas **15**, 122509 (2008).
[19] I. G. Abel, G. G. Plunk, E. Wang, M. Barnes, S. C. Cowley, W. Dorland, and A. A. Schekochihin, Rep. Prog. Phys. **76**, 116201 (2013).
[20] M. N. Rosenbluth and P. J. Catto, Nucl. Fusion **15**, 573 (1975).